

Collective excitations of a trapped boson-fermion mixture across demixing

P. Capuzzi, A. Minguzzi, and M. P. Tosi

NEST-INFM and Classe di Scienze, Scuola Normale Superiore, Piazza dei Cavalieri 7, I-56126 Pisa, Italy

We calculate the spectrum of low-lying collective excitations in a mesoscopic cloud formed by a Bose-Einstein condensate and a spin-polarized Fermi gas as a function of the boson-fermion repulsions. The cloud is under isotropic harmonic confinement and its dynamics is treated in the collisional regime by using the equations of generalized hydrodynamics with inclusion of surface effects. For large numbers of bosons we find that, as the cloud moves towards spatial separation (demixing) with increasing boson-fermion coupling, the frequencies of a set of collective modes show a softening followed by a sharp upturn. This behavior permits a clear identification of the quantum phase transition. We propose a physical interpretation for the dynamical transition point in a confined mixture, leading to a simple analytical expression for its location.

PACS numbers: 03.75.Kk, 03.75.Ss, 67.60.-g

I. INTRODUCTION

After the achievement of Bose-Einstein condensation in alkali-atom gases, advanced techniques are being developed to cool gases of fermionic isotopes inside magnetic traps. Since the Pauli principle forbids s -wave collisions between spin-polarized fermions, to reach the degeneracy regime in the fermionic case one must resort to collisions against a distinguishable species, either bosonic or fermionic [1]. Boson-fermion mixtures are currently being produced and studied in several experiments [2, 3, 4, 5, 6, 7].

Starting from the work on strongly interacting ^3He - ^4He liquids, cold mixtures have played an important role in the development and testing of the theory of quantum phase transitions. In this context trapped mixtures of atomic gases offer a unique opportunity due to their high diluteness. Mixtures of a Bose-Einstein condensate and a degenerate Fermi gas are predicted to have a rich phase diagram. In the case of attractive boson-fermion interactions, where the boson-fermion overlap is largest, the boson-induced fermion-fermion attraction may lead to the formation of a superfluid state [8]. In the case of repulsive interactions, on the other hand, the system is expected to undergo spatial separation when the repulsions overcome the kinetic energy [9]. The conditions for demixing have been derived for a homogeneous mixture [10] and also in the experimentally relevant case of a mixture under harmonic confinement [11, 12, 13]. The static equilibrium properties of such mixtures across phase separation and the topology of the particle density profiles in the demixed state have been studied [14]. Of course, the transition to the demixed state in a mesoscopic cloud under confinement is spread out as the overlap energy between its two components reaches a maximum and then gradually decreases on further increase of the boson-fermion coupling.

In the mixed state the dynamical properties of a boson-fermion mixture have been investigated both for a homogeneous system [15] and in a mesoscopic cloud under external harmonic confinement [16]. The purpose of the

present paper is to follow the dynamics of a harmonically confined cloud with increasing boson-fermion repulsion and to look for a signature of the transition to spatial separation in the spectrum of collective modes. We focus here on the study of the dynamics in the collisional regime, which at high temperature has already been reached in some experiments [7] and can be attained at low temperature in the presence of impurities [17]. We solve the hydrodynamic equations beyond the Thomas-Fermi approximation, including surface effects which are crucial for a proper description of particle density fluctuations as the cloud approaches demixing.

The paper is organized as follows. In Sec. II we introduce the specific system that we study and the hydrodynamic equations which we use throughout the paper. Section III discusses the equilibrium density profiles that are needed to evaluate the collective modes of the mixture in Sec. IV. Finally, Sec. V presents a summary of our results and an outlook towards future developments.

II. THEORETICAL MODEL

We consider a dilute fluid composed by two species of alkali atoms, one fermionic and the other bosonic in a Bose-Einstein condensed state, confined inside a spherical trap at zero temperature. The interactions between the bosons and between bosons and fermions are described by contact potentials and are parametrized by the coupling constants $g_{BB} = 4\pi\hbar^2 a_{BB}/m_B$ and $g_{BF} = 2\pi\hbar^2 a_{BF}/m_r$ in terms of the s -wave scattering lengths a_{BB} and a_{BF} and of the masses m_B and m_F of each species, with $m_r = (1/m_B + 1/m_F)^{-1}$ being the reduced mass. The fermions are spin-polarized and are taken as noninteracting, since collisions in the s -wave channel are forbidden by the Pauli principle. In the following we have chosen $g_{BB} > 0$ and $g_{BF} > 0$, as for the ^6Li - ^7Li mixture studied in the experiments of Schreck *et al.* [2].

We describe the dynamics of the system by starting from the equations of generalized hydrodynamics [18] for the particle densities $\rho_\sigma(\mathbf{r}, t)$ and the current densities

$\mathbf{j}_\sigma(\mathbf{r}, t)$, with $\sigma = B, F$. These equations read

$$\frac{\partial \rho_\sigma}{\partial t} + \nabla \cdot \mathbf{j}_\sigma = 0 \quad (1)$$

and

$$m_\sigma \frac{\partial \mathbf{j}_\sigma}{\partial t} + \nabla \cdot \Pi^\sigma + \rho_\sigma \nabla \tilde{V}_\sigma = 0. \quad (2)$$

Here, \tilde{V}_σ are the effective mean-field potentials and Π^σ are the kinetic stress tensors. In the dilute regime we may adopt the Hartree-Fock approximation for the effective potentials,

$$\tilde{V}_F = V_F^{ext} + g_{BF} \rho_B \quad (3)$$

and

$$\tilde{V}_B = V_B^{ext} + g_{BB} \rho_B + g_{BF} \rho_F, \quad (4)$$

where $V_\sigma^{ext} = m_\sigma \omega_\sigma^2 r^2 / 2$ are the (isotropic) external trapping potentials.

The above equations can be closed in the collisional regime, where we assume a local dependence of the stress tensors on the particle densities. In the dilute limit the Thomas-Fermi approximation yields the fermionic stress tensor as the local-density form of the tensor for the ideal Fermi gas. However, we have added to this Thomas-Fermi form a surface contribution in the form derived by von Weizsäcker [19], in order to avoid spurious divergences in the density fluctuations at the classical radius of the cloud. Thus, the form for Π_{ij}^F reads

$$\begin{aligned} \Pi_{ij}^F = & \frac{2}{5} A \rho_F^{5/3} \delta_{ij} - \frac{\hbar^2}{6 m_F} \left[\sqrt{\rho_F} \nabla_i \nabla_j \sqrt{\rho_F} \right. \\ & \left. - \nabla_i \sqrt{\rho_F} \nabla_j \sqrt{\rho_F} \right] \end{aligned} \quad (5)$$

where $A = \hbar^2 (6\pi^2)^{2/3} / 2m_F$. This choice is in agreement with the general structure of the fermionic stress tensor under harmonic confinement as demonstrated in Ref. [20]. In the same approximation the bosonic stress tensor has only the surface contribution

$$\Pi_{ij}^B = -\frac{\hbar^2}{2m_B} \left[\sqrt{\rho_B} \nabla_i \nabla_j \sqrt{\rho_B} - \nabla_i \sqrt{\rho_B} \nabla_j \sqrt{\rho_B} \right], \quad (6)$$

as can also be obtained from the Gross-Pitaevskii equation [21]. In Eqs. (5) and (6) we have left out velocity-dependent terms which do not enter linear dynamics.

Using Eqs. (3)-(6) for the effective potentials and the kinetic stress tensors we can rewrite the equations for the current densities as

$$m_\sigma \frac{\partial \mathbf{j}_\sigma}{\partial t} = \rho_\sigma (\mathbf{F}_\sigma - \nabla V_\sigma - g_{BF} \nabla \rho_{\bar{\sigma}}), \quad (7)$$

where $\bar{\sigma}$ denotes the component different from σ and for convenience we have introduced the forces

$$\mathbf{F}_B = -\nabla \left[g_{BB} \rho_B - \frac{\hbar^2}{2m_B} \frac{\nabla^2 \sqrt{\rho_B}}{\sqrt{\rho_B}} \right] \quad (8)$$

and

$$\mathbf{F}_F = -\nabla \left[A \rho_F^{2/3} - \frac{\hbar^2}{6m_F} \frac{\nabla^2 \sqrt{\rho_F}}{\sqrt{\rho_F}} \right]. \quad (9)$$

In these equations we shall set $\rho_\sigma(\mathbf{r}, t) = \rho_\sigma(r) + \delta\rho_\sigma(\mathbf{r}, t)$ and proceed first to discuss the equilibrium profiles $\rho_\sigma(r)$.

III. EQUILIBRIUM PROFILES AND SPATIAL SEPARATION

The particle density profiles at equilibrium are obtained by imposing the steady-state condition $\partial \mathbf{j}_\sigma / \partial t = 0$ in Eq. (7). This ensures consistence between static and dynamical solutions as well as fulfilment of the generalized Kohn theorem [22]. The above equilibrium condition is in fact equivalent to a minimization of the mean-field energy functional

$$\begin{aligned} E[\rho_F, \rho_B] = & \int d^3r \left(V_B \rho_B + \frac{g_{BB}}{2} \rho_B^2 + \xi_B \right) \\ & + \int d^3r \left(V_F \rho_F + \frac{3}{5} A \rho_F^{5/3} + \xi_F \right) \\ & + g_{BF} \int d^3r \rho_F \rho_B, \end{aligned} \quad (10)$$

where the quantum pressure or surface energy terms read

$$\xi_B = \frac{\hbar^2}{2m_B} |\nabla \sqrt{\rho_B}|^2 \quad (11)$$

and

$$\xi_F = \frac{\hbar^2}{6m_F} |\nabla \sqrt{\rho_F}|^2. \quad (12)$$

As was found in previous studies [9, 10, 11, 12], on increasing the boson-fermion repulsion the mixture undergoes spatial separation. In a finite cloud the transition is smooth and can be described by following the behavior of the boson-fermion interaction energy $E_{int} = g_{BF} \int d^3r \rho_B \rho_F$, which for a given coupling strength is determined by the overlap of the two species [13, 14]. The onset of the transition is signalled first by a decrease of E_{int} as a function of the boson-fermion coupling (partial separation), until the value E_{int} becomes negligible (full demixing). The maximum of the interaction energy as a function of g_{BF} has been estimated for harmonic confinement at zero temperature within the Thomas-Fermi approximation to lie at

$$\frac{a_{BF}^{part}}{a_{BB}} = \left(c_1 \frac{N_F^{1/2}}{N_B^{2/5}} + c_2 \frac{N_B^{2/5}}{N_F^{1/3}} \right)^{-1}, \quad (13)$$

where

$$\begin{aligned} c_1 = & \frac{15^{3/5}}{48^{1/2}} \frac{(m_F + m_B) m_F^{1/2}}{2 m_B^{3/2}} \left(\frac{a_{BB}}{d} \right)^{3/5} \\ c_2 = & \frac{48^{1/3}}{15^{3/5}} \left(\frac{6}{\pi} \right)^{2/3} \frac{m_F + m_B}{2 m_F} \left(\frac{a_{BB}}{d} \right)^{2/5} \end{aligned} \quad (14)$$

and $d = (\hbar/m_B\omega_B)^{1/2}$ is the bosonic harmonic-oscillator length. The point of full demixing as given by the Thomas-Fermi approximation occurs instead at

$$a_{BF}^{full} = \left(\frac{a_{BB}}{\alpha k_F} \right)^{1/2} \quad (15)$$

where $k_F = (48N_F)^{1/6}/d$ and $\alpha = [3^{1/3}/(2\pi)^{2/3}](m_F + m_B)^2/(4m_F m_B)$. As we shall see below, the analysis of the mode frequencies as functions of the boson-fermion coupling strength yields a dynamical condition for spatial separation which is intermediate between the two static conditions laid out in Eqs. (13) and (15).

IV. COLLECTIVE EXCITATION SPECTRUM

We proceed to evaluate the dynamical behavior of the cloud as it undergoes spatial separation. Under the assumption of a weak external drive we can neglect anharmonic contributions. The spectrum of collective excitations is then obtained by linearizing Eq. (7) around the equilibrium state. By taking the Fourier transform with respect to the time variable we thus obtain coupled eigenvalue equations for the density fluctuations $\delta\rho_\sigma$ of each species,

$$m_\sigma \Omega^2 \delta\rho_\sigma = \nabla \cdot (\rho_\sigma \delta\mathbf{F}_\sigma) - g_{BF} \nabla \cdot (\rho_\sigma \nabla \delta\rho_\sigma). \quad (16)$$

The expressions for the linearized forces $\delta\mathbf{F}_\sigma$ are given in Appendix A.

We have solved Eq. (16) in the case of a spherically symmetric confinement, setting the values of the trapping frequencies at $\omega_F = \omega_B = \omega_0$ with $\omega_0 = 2\pi \times 1000 \text{ s}^{-1}$ and the values of the boson-boson scattering length at $a_{BB} = 0.27 \text{ nm}$, which correspond to the ${}^6\text{Li}$ - ${}^7\text{Li}$ mixture in the Paris experiment [2, 23]. We vary the mutual scattering length a_{BF} and the number of particles of each species in order to explore the transition from the mixed state to the fully separated state. In particular, the choice $N_F = 10^4$ and $N_B = 2.4 \times 10^7$ leads to bosonic and fermionic clouds having approximately the same size at zero coupling.

The numerical procedure that we have used can be summarized as follows: (i) we look for a spherically symmetric steady-state solution of Eqs. (7)-(9) by a steepest-descent method [24, 25]; (ii) we decompose the density fluctuations into components of definite angular momentum, *i.e.* we factorize the amplitude of the fluctuations as $\delta\rho_\sigma(\mathbf{r}) = \delta\rho_\sigma^l(r) Y_{lm}(\hat{r})$ with Y_{lm} the spherical harmonic functions; and (iii) we set up an eigenvalue problem for each l by discretizing Eqs. (16) and solve it by means of standard routines from the LAPACK library [26].

The results for the frequencies of the monopole ($l = 0$) modes are given in Fig. 1 as functions of the boson-fermion coupling for $N_F = 10^4$ and various values of N_B . A sampling of the eigenvectors is reported in Fig. 2. We have labelled the modes as “fermionic” (dots) or

“bosonic” (circles) according to the nature of their eigenvalue in the limit of vanishing g_{BF} . Of course, at finite values of g_{BF} the modes are coupled and the labels are just conventional, but can still be assigned by looking at the nodes of each density fluctuation: fermionic (bosonic) modes keep a constant number of nodes in $\delta\rho_F$ ($\delta\rho_B$) with increasing g_{BF} .

A common feature of our results in Fig. 1 is a non-monotonic behavior of the frequency of the fermionic modes as the cloud evolves from the mixed regime to the fully separated one. With increasing g_{BF} a fermionic mode acquires the character of an out-of-phase fluctuation of the two components (see Fig. 2) and we observe a softening of its frequency. This we interpret as a signal of the approaching spatial-separation transition: with increasing boson-fermion repulsion the out-of-phase oscillation requires less and less energy, until at the transition the mixture takes as its equilibrium configuration a state which corresponds to a “frozen” out-of-phase oscillation. The nonzero value of the lowest mode frequency at the transition point appears to be due to the presence of the confinement, since in a linearized theory it should tend to zero in the proper thermodynamic limit.

The transition point as dynamically determined by the sharp upturn in the fermionic mode frequencies does not agree with the static criterion (13) or (15), but corresponds to an intermediate point where the equilibrium density of the fermionic cloud vanishes at the center of the trap (see the dotted lines in Fig. 2). In the limit of large number of bosons this point can be analytically estimated within the Thomas-Fermi approximation to be

$$\frac{a_{BF}^{dyn}}{a_{BB}} = \frac{2m_F}{m_B + m_F} \frac{\mu_F}{\mu_B} \quad (17)$$

where μ_F and μ_B are the chemical potentials for fermions and bosons, respectively. In a local-density picture this corresponds to a minimum in the velocity of the fermionic sound wave. The locations of the transition point according to the criterion in Eqs. (13) and (17) are shown by the arrows in Fig. 1.

On further increasing the boson-fermion coupling in the spatially separated regime we observe that the frequency of the fermionic modes continues to increase. This can be understood by means of a simple model of sound-wave propagation inside a uniform shell of given thickness η . The velocity c_s of the wave is related to the compressibility κ of the fermionic gas according to $c_s = (m_F \rho_F \kappa)^{-1/2}$ and by imposing rigid boundary conditions at the edges of the shell we can obtain its frequency spectrum. For $l = 0$ the lowest sound mode is given by [27]

$$\Omega_{\text{SW}} = \frac{\pi c_s}{\eta} \quad (18)$$

and the sound velocity can be estimated from the ideal-

gas expression of the pressure ($p = \frac{2}{5} A \rho_F^{5/3}$) as

$$c_s^2 = \frac{2}{3} \frac{A}{m_F} \rho_F^{2/3}. \quad (19)$$

Since we are assuming a constant-density shell for each value of a_{BF} , to actually compare the predictions of Eq. (18) with the numerical results in Fig. 1 we need a suitable choice of the effective fermionic density ρ_F . In Fig. 3 we show the frequency of the lowest sound mode calculated from Eq. (18) as a function of a_{BF} using two choices for the effective density, one corresponding to the maximum value of the fermionic equilibrium profile and the other evaluated for a uniform spherical shell with the same number of fermions and the radii taken from the Thomas-Fermi equilibrium profile. In view of the rough approximations that we are making, the agreement in Fig. 3 between the numerical calculation of the lowest monopole frequency and this simple model is quite satisfactory. Such a degree of quantitative agreement is not found for the high-frequency modes, since the density fluctuation tails become more marked and are more sensitive to the inhomogeneity of the fermionic shell.

Returning to Fig. 1, it also shows that the frequencies of the bosonic monopole modes are essentially unaffected by the boson-fermion interaction. This is due to the fact that with our choice of system parameters the bosonic cloud has a considerably higher density than the fermionic one, leading to a weakly coupled dynamics. It is worth recalling that this is at present a relevant experimental situation, with the fermionic cloud containing a denser Bose-Einstein condensate.

We have also examined the case of comparable numbers of bosons and fermions (see Fig. 4). In this case the frequency of the low-lying bosonic monopole modes increases slowly with increasing boson-fermion coupling while the frequency of the fermionic ones is quite unchanged except for level crossings (left panel in Fig. 4). The dipolar ($l = 1$) modes show similar features (right panel). The behavior found for the higher modes, *e.g.* those with frequencies larger than approximately $7\omega_0$, is instead similar to that shown in Fig. 1 and is therefore not reported in Fig. 4. These features can be understood by considering the relative size of the two clouds: the hole produced in the fermionic cloud by the bosons is in this case so small that the low-lying fermionic fluctuations cannot sense it.

Finally, we have solved the hydrodynamic equations for the $l = 1$ dipolar oscillations with a choice of particle numbers analogous to that made for the monopole modes in Fig. 1. As is shown in Fig. 5, in this case the lowest fermionic-mode frequency initially decreases monotonically and tends to a constant value for large values of g_{BF} . In addition, we find the Kohn mode at the frequency of the trap for any value of the boson-fermion coupling. The higher modes exhibit instead the same behavior as the monopole modes in Fig. 1.

V. SUMMARY AND CONCLUDING REMARKS

In summary, in this paper we have studied how the mutual repulsive interactions affect the spectrum of collective excitations in a trapped boson-fermion mixture in the collisional regime as the mixture undergoes spatial separation. For this purpose we have derived and solved the equations of generalized hydrodynamics beyond the Thomas-Fermi approximation, by including surface density-gradient terms in the form first proposed by von Weizsäcker. When the two component clouds have similar sizes (implying $N_B \gg N_F$), we have found that the frequencies of the fermionic $l = 0$ modes decrease as the boson-fermion scattering length is increased and the mixture approaches demixing. This frequency softening is directly related to the change in shape of the equilibrium density profiles as the repulsive interactions become stronger and reflects the tendency of the two components to spatially separate. At the point where the fermions are expelled from the center of the trap, although the two clouds still partially overlap, the fermionic mode frequencies start to grow in a fashion which essentially agrees with a simple model of sound wave propagation inside a fermionic spherical shell. A similar trend is also found in the frequencies of the fermionic $l = 1$ bulk modes, while the bosonic dipolar surface mode displays the Kohn-theorem behavior and is therefore unaffected by the interactions. All these features are very different from those that we observe for $N_B \simeq N_F$, when the bosonic modes are the most sensitive to the boson-fermion coupling.

We have thus found a clear dynamical signature of the onset of spatial demixing in the spectrum of collective modes in the case $N_B \gg N_F$. This is expected to be helpful since the formation of a symmetric “egg” configuration in the demixed cloud is not easily detected from an analysis of column density profiles [13]. The dynamical condition for demixing is given by the point where the topology of the fermionic equilibrium density profile changes as the fermions start to arrange themselves in a shell around the bosons. This point does not coincide with the points of partial or full demixing as obtained from the static study of the boson-fermion energy functional. However, this is easily understood if one considers that in a finite system the transition is smooth and can be characterized by several different conditions, which will coincide only in the thermodynamic limit.

The present analysis can be extended to study the transition towards “exotic” configurations of the demixed cloud, as predicted by the static study of the energy functional [14]. A calculation of the spectrum of collective excitations of a boson-fermion mixture across spatial separation in the collisionless regime is in progress and will be reported elsewhere.

Acknowledgments

This work was supported by INFM through the PRA-Photonmatter Program.

APPENDIX A: FULL EXPRESSIONS FOR FORCE FLUCTUATIONS

As was mentioned in the text, we decompose the particle density fluctuations in their angular-momentum com-

ponents as $\delta\rho_\sigma(\mathbf{r}) = \delta\rho_\sigma(r) Y_{lm}(\hat{r})$. Then, for each l we calculate $\delta\mathbf{F}_\sigma = \mathbf{F}_\sigma[\rho_\sigma(r) + \delta\rho_\sigma(r) Y_{lm}(\hat{r})] - \mathbf{F}_\sigma[\rho_\sigma(r)]$ to linear terms in the density fluctuations. This yields

$$\delta\mathbf{F}_F = -\nabla \left\{ \left[\frac{2}{3} A \rho_F^{-1/3} \delta\rho_F + \frac{\hbar^2}{6 m_F} \left(\frac{\rho'_F}{r \rho_F^2} + \frac{\rho''_F}{2\rho_F^2} - \frac{\rho_F'^2}{2\rho_F^3} + \frac{l(l+1)}{r^2 \rho_F} \right) \delta\rho_F - \frac{\hbar^2}{6 m_F} \left(\frac{1}{r \rho_F} - \frac{\rho'_F}{2\rho_F^2} \right) \delta\rho'_F - \frac{\hbar^2}{12 m_F \rho_F} \delta\rho''_F \right] Y_{lm} \right\} \quad (\text{A1})$$

and

$$\delta\mathbf{F}_B = -\nabla \left\{ \left[g_{BB} \delta\rho_B + \frac{\hbar^2}{2 m_B} \left(\frac{\rho'_B}{r \rho_B^2} + \frac{\rho''_B}{2\rho_B^2} - \frac{\rho_B'^2}{2\rho_B^3} + \frac{l(l+1)}{r^2 \rho_B} \right) \delta\rho_B - \frac{\hbar^2}{2 m_B} \left(\frac{1}{r \rho_B} - \frac{\rho'_B}{2\rho_B^2} \right) \delta\rho'_B - \frac{\hbar^2}{4 m_B \rho_B} \delta\rho''_B \right] Y_{lm} \right\}. \quad (\text{A2})$$

In these equations a prime means a derivative with respect to r .

-
- [1] B. DeMarco and D. S. Jin, *Science* **285**, 1703 (1999).
 - [2] F. Schreck, L. Khaykovich, K. L. Corwin, G. Ferrari, T. Bourdel, J. Cubizolles, and C. Salomon, *Phys. Rev. Lett.* **87**, 080403 (2001).
 - [3] J. Goldwin, S. B. Papp, B. DeMarco, and D. S. Jin, *Phys. Rev. A* **65**, 021402 (2002).
 - [4] Z. Hadzibabic, C. A. Stan, K. Dieckmann, S. Gupta, M. W. Zwierlein, A. Görlitz, and W. Ketterle, *Phys. Rev. Lett.* **88**, 160401 (2002).
 - [5] G. Roati, F. Riboli, G. Modugno, and M. Inguscio, *Phys. Rev. Lett.* **89**, 150403 (2002).
 - [6] G. Modugno, G. Roati, F. Riboli, F. Ferlaino, R. J. Brecha, and M. Inguscio, *Science* **297**, 2240 (2002).
 - [7] F. Ferlaino, R. J. Brecha, P. Hannaford, F. Riboli, G. Roati, G. Modugno, and M. Inguscio, *cond-mat/0211051*.
 - [8] M. J. Bijlsma, B. A. Heringa, and H. T. C. Stoof, *Phys. Rev. A* **61**, 053601 (2000); D. V. Efremov and L. Viverit, *Phys. Rev. B* **65**, 134519 (2002).
 - [9] K. Mølmer, *Phys. Rev. Lett.* **80**, 1804 (1998); N. Nygaard and K. Mølmer, *Phys. Rev. A* **59**, 2974 (1999).
 - [10] L. Viverit, C. J. Pethick, and H. Smith, *Phys. Rev. A* **61**, 053605 (2000).
 - [11] A. Minguzzi and M. P. Tosi, *Phys. Lett. A* **268**, 142 (2000).
 - [12] T. Miyakawa, K. Oda, T. Suzuki, and H. Yabu, *J. Phys. Soc. Jpn.* **69**, 2779 (2000).
 - [13] Z. Akdeniz, P. Vignolo, A. Minguzzi, and M. P. Tosi, *J. Phys. B* **35**, L105 (2002).
 - [14] Z. Akdeniz, A. Minguzzi, P. Vignolo, and M. P. Tosi, *Phys. Rev. A* **66**, 013620 (2002).
 - [15] S. K. Yip, *Phys. Rev. A* **64**, 023609 (2001).
 - [16] T. Miyakawa, T. Suzuki, and H. Yabu, *Phys. Rev. A* **62**, 063613 (2000); T. Miyakawa, T. Suzuki, and H. Yabu, *ibid.* **64**, 033611 (2001); P. Capuzzi and E. S. Hernández, *ibid.* **64**, 043607 (2001); T. Sogo, T. Miyakawa, T. Suzuki, and H. Yabu, *ibid.* **66**, 013618 (2002); P. Capuzzi and E. S. Hernández, *J. Low. Temp. Phys.* **126**, 425 (2002).
 - [17] M. Amoruso, I. Meccoli, A. Minguzzi, and M. P. Tosi, *Eur. Phys. J. D* **8**, 361 (2000).
 - [18] N. H. March and M. P. Tosi, *Ann. Phys. (NY)* **81**, 414 (1973).
 - [19] C. F. von Weizsäcker, *Z. Phys.* **96**, 431 (1935).
 - [20] A. Minguzzi, P. Vignolo, and M. P. Tosi, *Phys. Rev. A* **63**, 063604 (2001).
 - [21] A. Minguzzi, M. L. Chiofalo, and M. P. Tosi, *Phys. Lett. A* **236**, 237 (1997).

- [22] E. Zaremba and H. C. Tso, Phys. Rev. B **49**, 8147 (1994); J. F. Dobson, Phys. Rev. Lett. **73**, 2244 (1994).
- [23] Regarding the choice of the traps we have set the bosonic and fermionic frequencies equal, taking the geometrical average of the experimental values in the three Cartesian directions.
- [24] W. H. Press, S. A. Teukolsky, W. T. Vetterling, and B. P. Flannery, *Numerical Recipes in Fortran 77: The Art of Scientific Computing* (Cambridge University Press, Cambridge, 1992).
- [25] F. Dalfovo and S. Stringari, Phys. Rev. A **53**, 2477 (1996).
- [26] E. Anderson, Z. Bai, C. Bischof, S. Blackford, J. Demmel, J. Dongarra, J. Du Croz, A. Greenbaum, S. Hammarling, A. McKenney, et al., *Lapack User's Guide* (1999), URL <http://www.netlib.org/lapack>.
- [27] This is readily obtained by imposing rigid boundary conditions on the lowest $l = 0$ solution for sound-wave propagation inside a uniform spherical shell with hard walls. The wave is described by a spherical Bessel function j_0 of appropriate argument.

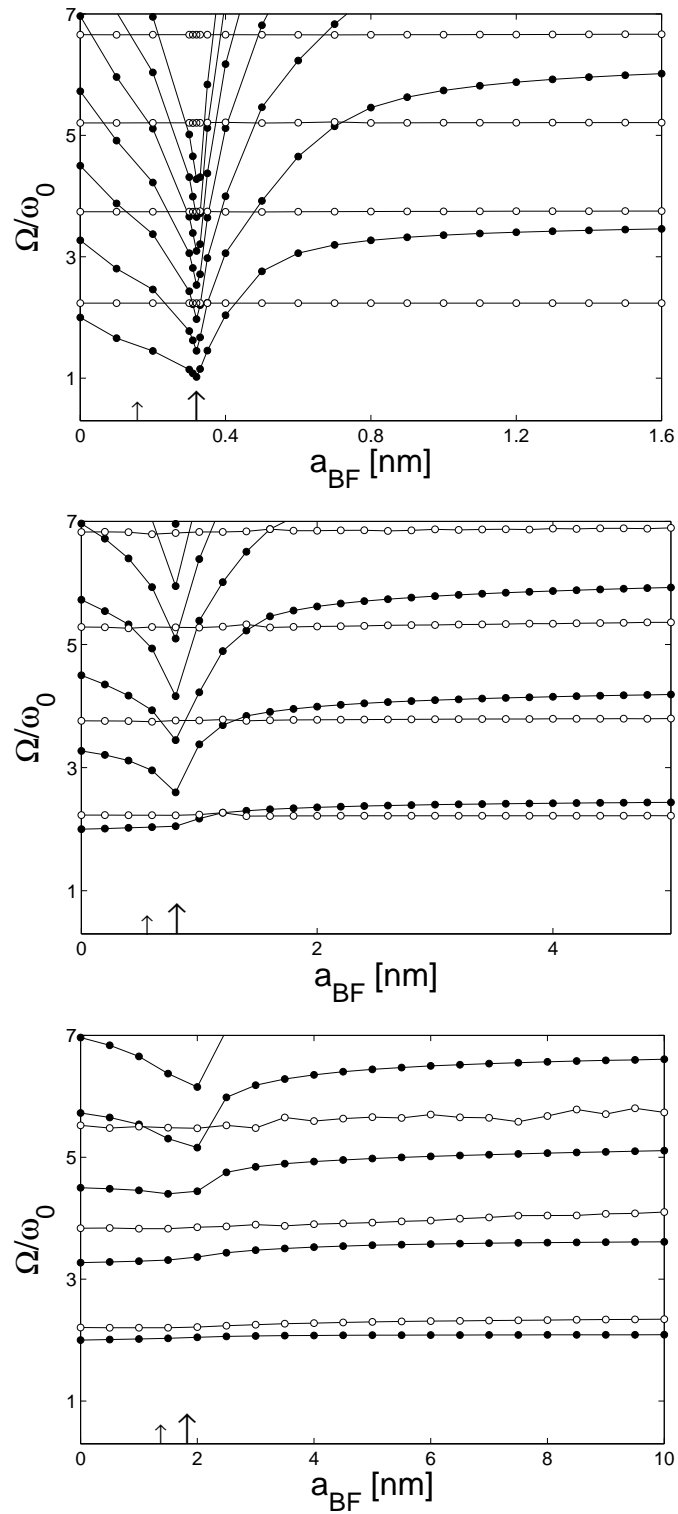


FIG. 1: Frequencies of $l = 0$ collective modes (in units of the trap frequency ω_0) as functions of the boson-fermion scattering length a_{BF} (in nm). The panels from top to bottom correspond to $N_B = 2.4 \times 10^7, 10^6$, and 10^5 bosons. Each frame displays the low-lying hydrodynamic modes (fermionic – dots and bosonic – open circles) from the numerical solution of Eq. (16) with $N_F = 10^4$ fermions and the other parameters as specified in the text. In each panel the small arrow indicates the onset of partial demixing from a static criterion (Eq. (13)) and the large arrow indicates the point of vanishing fermionic density at the center of the trap (Eq. (17)). The lines are a guide to the eye.

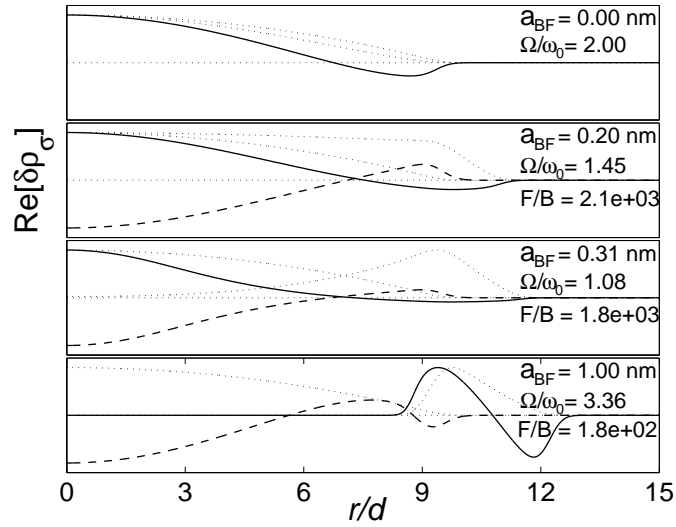


FIG. 2: Monopolar density fluctuation profiles (arbitrary units) as functions of the radial coordinate (in units of the harmonic oscillator length d) for various values of the boson-fermion coupling as indicated in the panels, with $N_B = 2.4 \times 10^7$ and $N_F = 10^4$. Continuous and dashed lines display the fermionic and bosonic profiles, respectively. The scale of each fluctuation has been changed to fit in the graph (F/B indicates the ratio between the maximum value attained by the fermionic and bosonic fluctuation profiles). The dotted lines show the equilibrium density profiles, again rescaled to fit in the graph.

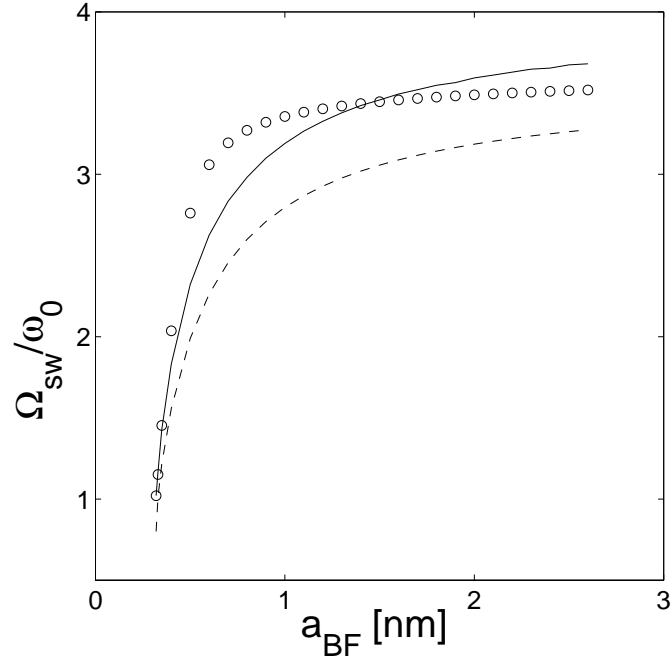


FIG. 3: Frequency of the lowest fermionic monopole mode after demixing, as a function of a_{BF} (in nm) for $N_B = 2.4 \times 10^7$ and $N_F = 10^4$. The circles are from the numerical solution of Eq. (16), while the lines show the predictions of Eq. (18) taking as effective density the maximum value of the equilibrium density (full line) or the density of a uniform shell with $N_F = 10^4$ fermions inside the Thomas-Fermi radii (dashed line).

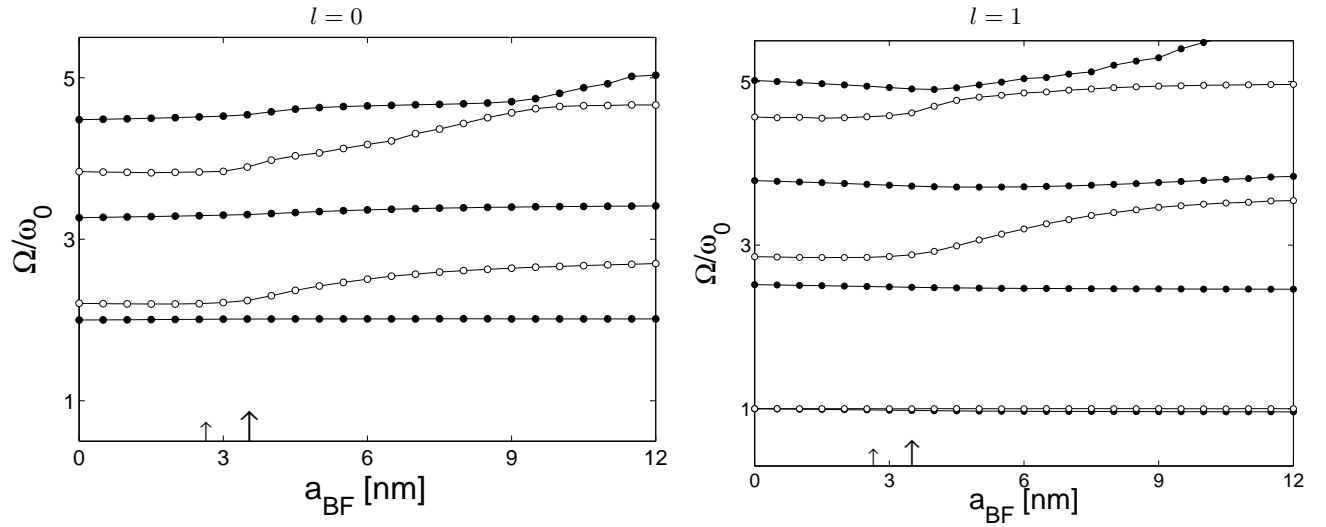


FIG. 4: Frequencies of the $l = 0$ (left panel) and $l = 1$ (right panel) collective excitations (in units of the trap frequency ω_0) as functions of a_{BF} (in nm) for the case $N_B = N_F = 10^5$. The symbols and the system parameters are as in Fig. 1.

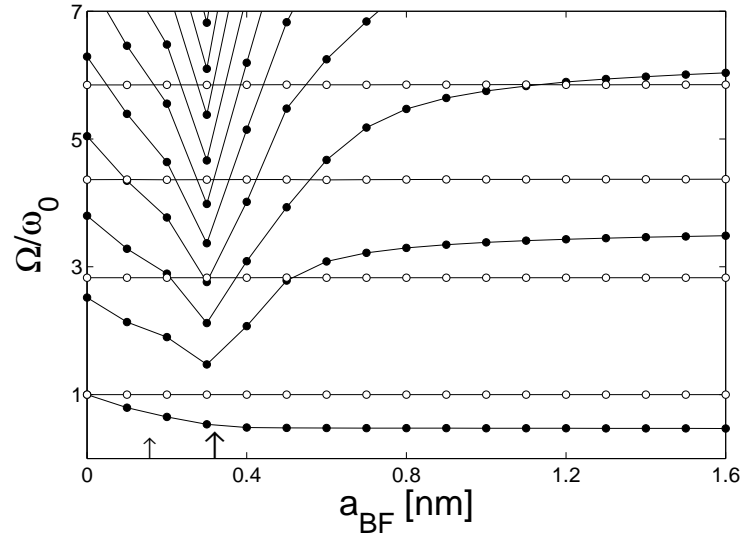


FIG. 5: Frequencies of the $l = 1$ modes (in units of the trap frequency ω_0) as functions of a_{BF} (in nm) for $N_B = 2.4 \times 10^7$ and $N_F = 10^4$. The symbols and the system parameters are as in Fig. 1.